Effect of the Cross-linking Density for the Gold Core Oxidation in Thermo- and pH- Responsive Hybrid Au@pNIPAM and Au@p4VP Systems

Manuel Doña,[1] Carlos Alarcon-Fernández,[1] Juan Manuel López-Romero,[1] Rafael Contreras-Cáceres*[1,2]

[1] Department of Organic Chemistry, Faculty of Sciences, University of Malaga, 29071, Malaga, Spain

[2] Complutense University of Madrid, Faculty of Pharmacy. Department of Chemistry of Pharmaceutical Science, Plaza Raman y Cajal, Madrid 28040, Spain

Abstract

Here we report on a detailed study that concerns the oxidation of spherical gold nanoparticles (AuNPs) encapsulated into thermo- and pH-responsive microgels. Initially, two types of hybrid systems structured as spherical 50 nm gold nanoparticles coated with a thermo-responsive (N-iIsopropylacrylamide) or a pH-responsive (4-vinylpyridine) microgel are fabricated. Janus nanoparticles are obtained in case of p4VP systems. Then, a gradual gold elimination is achieved introducing each nanohybrid system into a mixture of cetyltrimethylammonium bromide (CTAB) and gold chloride ($HAuCl_4$), thus obtaining hollow colloidal structures ~~with potential application in controlled drug delivery~~. The synthesis of Au@pNIPAM and Au@p4VP systems is performed at different crosslinking densities (5, 10 and 15%), and the decrease in the gold plasmon absorption band with the oxidation time is monitored at the two possible microgel states (swollen and collapsed). Two parameters are determined, the Au core

etching rate and the molecule diffusion coefficient ($AuCl_4$/CTAB complex). This investigation offers the possibility to fabricate thermo- and pH-responsive hollow microgels that can be used for biomedical applications for controlled drug delivery purposes upon change in temperature or pH.

1. Introduction

The fabrication of hollow colloidal structures at the nanoscale level is an attractive approach for the encapsulation of a series of molecules or biomolecules, as enzymes, drugs, pesticides, contaminants, proteins or nucleic acids.[1, 2, 3] Due to their dimension, hollow nanoparticles can act as vehicles (microcontainers or microcapsules) in the transport of specimens into the organism to reach certain targets[4]. Concerning drug incorportion, microgels, which are defined as a cross-linked polymeric particle that remains dispersed in certain fluid, have been extensively reported as colloidal dispersions that have been used in the incorporation of, among others, several chemotherapeutic drugs, as fluorouacil, doxorubicin, paclitaxel, oxaliplatin.[5, 6, 7, 8, 9]. Compare with other colloidal nanoparticles utilized for the encapsulation and delivery of drugs, as polymers, liposomes, vesicles, micelles or dendrimers, microgels possess high stability and degree of flexibility, however, the most important advantage of microgels is the ability to respond to changes in the external environment, as temperature[10], pH[11], solvent nature[12], ionic strength[13] or visible light[14]. Specifically, a small variation in one of these parameters produces that a microgel remains in two different states, denoted as swollen and collapsed states. The transition between both states is known as volume phase transition (VPTT) or simply, phase transition. Two microgels widely investigated in colloidal chemistry are pNIPAM and p4VP[15, 16], which possess thermo- and pH-responsive capabilities, respectively. The former has a volume phase transition temperature at about 32ºC in water. Below this temperature, the

microgel network forms hydrogen bonds between acrylamide groups and water molecules, thus remaining in a swollen state. Above this temperature, hydrogen bonds are broken, and hydrophobic forces induce to water molecules come out from the microgel network, resulting in a collapse state. Concerning p4VP, it has a phase transition at pH 4.8. Below this pH value the nitrogen atom in pyridine groups are protonated, and the repulsive electrostatic contribution induces the microgel to swells. Above pH 4.8, the protonated nitrogen is neutralized, and the hydrophobic contribution of the vinyl groups results in a polymer collapse. Is important to mention that both microgels are prepared by free radical polymerization in presence of a crosslinker molecule, which is a compound with two terminal double bonds, as *N,N′*-methylenebisacrylamide, divinylbenzene or ethyleneglycol dimethacrylate[17, 18]. This easy and reproducible synthesis produces pure microgels that have been used in the encapsulation, transport and delivery of several drugs.[6,9] However, compare with "solid" microgels hollow structures are more interesting in terms of drug accumulation and release due the higher loading capacity produced by the hollow structure. [19, 20]. During the last years, the fabrication of hollow colloidal nanostructures has been achieved by using several strategies.[21] The most general approach consist in the encapsulation of particles acting as a core (gold, silica or polystyrene) with a microgel shell, thus creating a hybrid core@shell system[22, 23, 24, 25, 26, 27, 28]. A subsequent core elimination results in the fabrication of a stable hollow colloidal structure. Concerning thermos-responsive pNIPAM, several protocols have been reported. For example, Fu et al. synthesized hollow pNIPAM particles by HF treatment of previously synthesized SiO_2@pNIPAM particles.[22] Hydropropylcellulose (HPC) was used as core for the fabrication of hollow structures, this organic nuclei was removed by NaOH treatment.[20] Lyon et al. reported the fabrication of hollow pNIPAM nanoparticles by etching the Au

core with KCN from previously fabricate Au@pNIPAM particles.[25] These authors, apart from the synthesis and characterization of the hollow ~~stucturesstructures~~, they investigated the Au core etching rate above and below 32ºC in function of the polymer shell thickness and composition. More recently, the influence of the cross-linking density on the thermo-responsive behavior of fabricated hollow pNIPAM microgels has been reported[29]. In this case, the selective oxidation of the Au core was achieved by addition of $AuCl_4^-$ ions to an aqueous dispersion of Au@pNIPAM particles in presence of CTAB[30]. It was demonstrated that due to the relationship between crosslinker amount into the polymeric network and microgel elasticity, the final hollow structure depended on the crosslinking density inside the microgel network. However, a more detailed investigation about the diffusion of the Au^{3+}-CTAB complex into the microgel network as well as the gold etching rate in function of the cross-linking density in the this Au@pNIPAM system is highly desired.

Concerning pH-responsive hollow structures, not too many approaches have been reported. Hollow capsules were synthesized by layer by layer assembly of weak polyelectrolytes as poly(4-vinylpyridine) (P4VP) and poly(methacrylic acid) (PMA) onto SiO_2 particles. Eisenberg et al. used biamphiphilic triblock copolymers with polystyrene core for the synthesis of pH-triggered pH-responsive vesicles.[31] It is important to mention that we have recently reported the encapsulation of an anticancer molecule (paclitaxel) into hollow p4VP microgels for enhance the drug chemotherapeutic efficacy of this molecule in lung and breast cancer cell lines. This hollow system was also prepared by oxidizing the Au core by an Au^{3+}-CTAB mixture in a previously prepared Au@p4VP system.[32] More recently, we have also reported the fabrication of Au@p4VP particles with different shell thickness and cross-linker densities, which were used for the encapsulation and detection of Doxorubicin.

Here we present a detailed investigation concerning the Au gold core oxidation in both Au@pNIPAM and Au@p4VP hybrid systems at several cross-linker densities and at the two microgel states (swollen and collapsed). Initially, the hybrid Au@pNIPAM and Au@p4VP structures were fabricated by free radical polymerization of monomers using vinyl-terminated 50 nm AuNPs as core at different cross-linking densities. Then, gold oxidation was performed by treatment with a $HAuCl_4$/CTAB mixture. The initial core@shell hybrid morphology as well as the final hollow structure was confirmed by transmission electron microscopy (TEM) analysis. Particle dimension in function of temperature and pH were monitored by dynamic light scattering (DLS) measurements. The Au core etching rate as well as the gold etchant diffusion through the microgel network was obtained by analyzing the decrease in the AuNP absorption plasmon band during Au oxidation.[25,33] Our results offer the possibility to fabricate thermo- and pH-responsive hollow nanostructures with controlled loading behavior to be used in the encapsulation of drugs for biomedical applications.

2. Experimental section

2.1 Materials

Cetyltrimethylammonium bromide (CTAB, ≥96%), 3-butenoic acid (97%), and N-isopropylacrylamide (NIPAM, 97%), 4-Vinylpyridine (4VP, 95%), were purchased from by Aldrich. Tetrachloroauric acid ($HAuCl_4 \cdot 3H_2O$) and trisodium citrate dihydrate were supplied by Sigma. *N,N′*-Methylenebisacrylamide (BA) was supplied by Fluka. 2,2′-Azobis(2-methylpropionamidene) dihydrochloride (V50) was purchased from Across Organics. All reactants were used without further purification. Water was purified using a Milli-Q system (Millipore).

2.2 Characterization

UV–vis spectra were recorded with an Agilent 8453 UV-vis spectrophotometer using a quartz cell with a length path of 1 cm. DLS measurements were carried out in a Zetasizer Nano S from Malvern Instruments, at a detection angle of θ = 173° and at a scattering q vector q=0.0264 nm^{-1}. For TEM imaging a JEOL JEM1400 TEM microscope operated at 100 KV was employed. 10 μL of each colloidal solution were dropped on 100 mesh copper TEM grids and left to dry.

2.3 Synthesis of vinyl-terminated Au 50 nm nanoparticles.

Initially, vinyl-functionalized spherical 50 nm AuNPs were prepared through a modification of the seeded-mediated approach. $HAuCl_4$ was used as gold precursor, CTAB as stabilizer and 3-Butenoic acid as reducing agent[34]. Briefly, seeds particles were obtained by mixing 35 mL of 15 nm citrate-stabilized Au nanoparticles (prepared by citrate reduction)[35] with 15 mL of 0.03 M CTAB aqueous solution. Then, a growth solution was prepared by adding 800 μL of butenoic acid to 50 mL of an aqueous solution containing 1 mM $HAuCl_4$ and 15 mM CTAB. Subsequently, 4.5 mL of the seed solution was added under gentle magnetic stirring at 70°C. After 10 min, the excess of butenoic acid and CTAB were removed by centrifugation at 4500 rpm during 30 min. The supernatant was discarded and the pellet was redispersed in 50 mL of 4 mM CTAB. This dispersion was again centrifuged at 4500 rpm for 30 min, and the final precipitate was redispersed in 10 mL of water containing 125 μL 5m CTAB.

2.4 Synthesis of Au@pNIPAM particles

The pNIPAM encapsulation was performed by free radical polymerization of NIPAM in presence of the previously synthetized vinyl-terminated AuNPs.[34, 36, 37] To do that, 10 mL of AuNPs was heated to 70°C under N_2 flow. Then, three different Au@pNIPAM systems were prepared containing a fixed amount of NIPAM monomer 0.1698 g (1.5

mmol, 100%) and with 3 different BA amounts; 11.7 mg (5 mol %), 23.4 mg (10 mol %), and 35.1 mg (15 mol %), respectively, under magnetic stirring (see scheme 1). After 15 min, the N_2 flow was removed and the polymerization was initiated with the addition of V50 (100 μL 0.1 M) in each case. After 7−10 min the reddish solution became turbid, and the reaction was allowed to proceed for 2h at 70 °C. After that, the mixture was cool down at room temperature under stirring. Finally, it was diluted with water (50 mL), centrifuged (30 min at 4500 rpm), and redispersed in water. The centrifugation and redispersion process was repeated 5 times.

2.5 Synthesis of Au@p4VP particles

The p4VP encapsulation was achieved by free radical polymerization of 4VP in presence of the previously synthesized vinyl-terminated AuNPs[38]. Briefly, 10 mL of Au colloidal dispersion was heated to 70°C under N_2 flow. Then, three different Au@p4VP systems were prepared containing a fixed amount of 4VP monomer 162 μL (1.5 mmol, 100%) and 3 different amounts of BA; 0.0117 g (5 mol %), 0.0234 g (10 mol %), and 0.0351 g (15 mol %), respectively, under magnetic stirring (see scheme 1). After 15 min, the N_2 flow was removed and the polymerization was initiated with the addition of V50 (100 μL 0.1 M) in each case. After 7−10 min the reddish solution became turbid, and the reaction was allowed to proceed for 2h at 70 °C. Then, when the mixture was cool down at room temperature, it was diluted with water to 50 mL, centrifuged at 30 min during 4500 rpm), and redispersed in water. This process was repeated 5 times.

2.6 Gold core oxidation

In all cases, gold core oxidation was achieved through the same procedure previously reported.[30,32,34] For Au@pNIPAM particles, Au oxidation was performed at two different temperatures (27 and at 50ºC), and for Au@p4VP microgels, it was carried out

at pH 2 and 6. Briefly, in a typical reaction, 5 mL of the Au@pNIPAM or Au@p4VP particles at [Au]= 0.5 mM was immersed in 5 mL of a solution containing CTAB (100mM) and $HAuCl_4$ (0.275 mM) at the desired conditions of temperature and pH under mild magnetic stirring (see scheme 1). The UV-vis spectra evolution was recorded in every case acquiring a spectrum each 20 min.

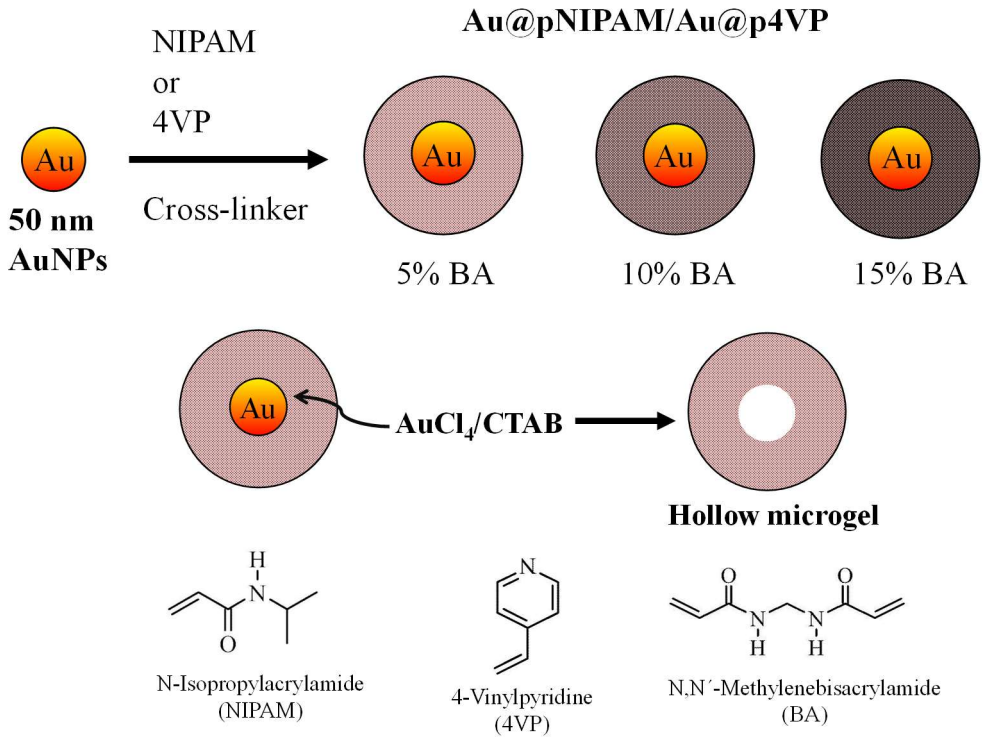

Scheme 1. Schematic representation for the synthesis of Au@pNIPAM and Au@4VP microgels using 5, 10 and 15% BA (up). Au core oxidation and fabrication of hollow microgels in presence of an $AuCl_4$/CTAB mixture (middle). Chemical structure of NIPAM, 4VP and BA (down).

3. Results and discussion

3.1 Fabrication of Au@pNIPAM and hollow pNIPAM particles.

Hollow thermos-responsive microgels were obtained by gold core oxidation using core@shell Au@pNIPAM hybrid particles as seeds. The initial system was structured

as 50 nm spherical Au core encapsulated by a pNIPAM shell. The microgel porosity allows diffuse the $AuCl_4$/CTAB complex through the microgel network towards the gold core surface. In order to vary the network porosity we have prepared microgels with different cross-linker densities. Wit this we can modify the $AuCl_4$/CTAB diffusion. As was previous reported,[30] the equilibrium constant to oxidize Au^o with $AuCl_4^-$ to $AuCl_2^-$ is extremely low. The presence of Br^- ions alters the redox potentials, and allows the oxidation of Au^o to $AuCl_2^-$ (See equation 1).

$$AuCl_4^- + 2Au^o + 2Cl^- = 3AuCl_2^- \quad [1]$$

The core@shell nature of the hybrid particles was confirmed by TEM analysis. Figure 1 includes representative TEM images for Au@pNIPAM systems at 5%, 10% and 15% BA, respectively. As is observed, the hybrid system was structured by an Au core which is surrounded by a polymer shell. A high contrast of Au spheres coated by a low contrast mono-dispersed polymer shell is observed. Table 1 includes the hydrodynamic diameter measured by DLS at both microgel states (swollen and collapsed) and at 3 different cross-linking densities. For Au@pNIPAM, the final particle size below 32ºC depends on the cross-linking amount into the microgel network. The hydrodynamic diameter decrease from 460 nm for 5% BA to 435 and 412 nm at 10 and 15% BA, respectively. This dependence can be extracted from Flory´s theory[39]. This theory stablish that in a microgel, the macroscopic swelling-deswelling behavior is determined by the balance of a mixture, elastic and ionic osmotic component (Π_{mix}, Π_{ela} and Π_{ion}, respectively). A polymer with a low cross-linking density has a more intense phase transition due to a lower elastic component, thus swelling in a higher extension. At 50ºC, pNIPAM is in a collapsed state due to water molecules are expelled from the microgel network. In this situation the measured hydrodynamic diameter was similar at the 3 different cross-linking densities (~210 nm).

As mentioned, the microgel porosity allows the $AuCl_4$/CTAB diffusion through the polymer network till reach the gold surface. Figure 2 includes TEM images of Au@pNIPAM at 10% BA after total gold oxidation. Is important to rmark that both no residual gold is observed into the microgels, and the hollow is located at the center of the microgel, thus supporting a homogeneous $AuCl_4$/CTAB diffusion through the microgel network.

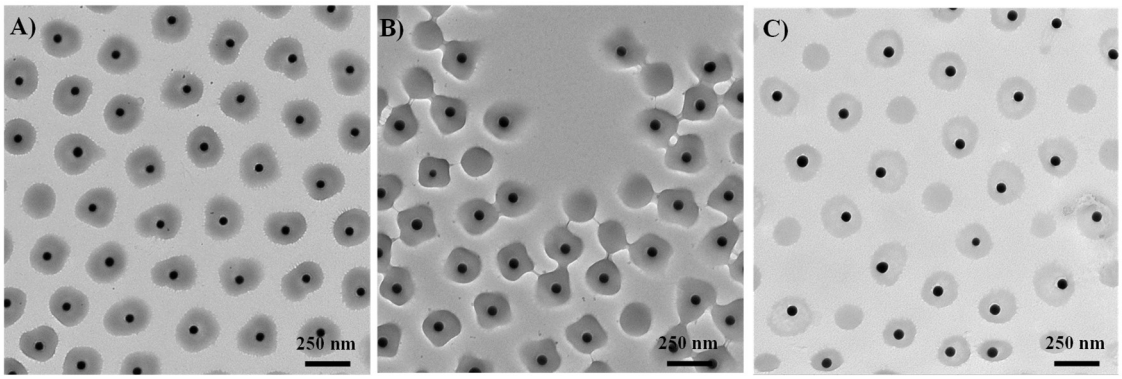

Figure 1. Representative TEM images of the Au@pNIPAM at A) 5%, B) 10% and C) 15% BA.

Table 1. Hydrodynamic diameter for Au@pNIPAM and Au@p4VP systems containing 5, 10 and 15% BA at the swollen and collapsed state

System	5%	10%	15%
Au@pNIPAM 25ºC	460	435	412
Au@pNIPAM 50ºC	210	210	210
Au@p4VP pH 2			
Au@p4VP pH 7			

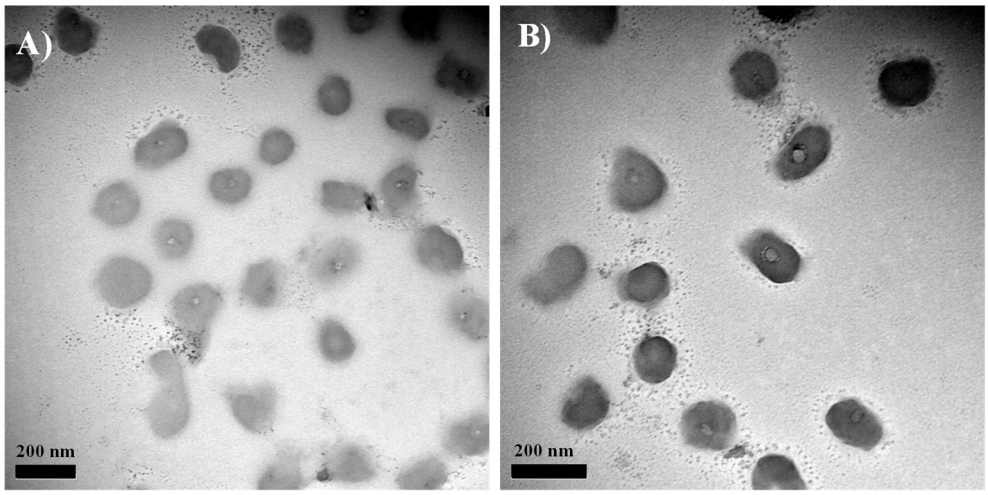

Figure 2. Representative TEM images of hollow pNIPAM particles at 10% BA

3.2 Gold etching rate and $AuCl_4$/CTAB coefficient diffusion

It is well-known that noble metal nanoparticles possess a localized surface plasmon band in the visible region. Consequently, the gold elimination can be monitored by UV-vis spectroscopy in all systems. Figure S1 shows time evolution of the UV-vis absorption spectrum during Au oxidation for Au@pNIPAM with 5%, 10% and 15% BA at 27ºC (swollen state). Initially, the UV-vis spectrum shows two principal peaks, which correspond to the localized surface plasmon band for Au@pNIPAM, located at about 535 nm, and the absorption band for the Au^{3+}/CTAB complex centered at ~400 nm. The decrease in the plasmon band intensity with time confirms a metal core oxidation, which reduces the Au particle size till total core elimination. As shown, the total oxidation is produced at about 300 minutes of reaction in all cases. Figure 3A represents the decrease of the normalized plasmon band absorbance with respect to oxidation time for the 3 different cross-linking percentages, 5% (black square), 10% (red circles) and 15% (blue triangles). As expected, Au oxidation dependeds on the cross-linker percentage within the microgel network, a decrease in the BA content results in a less

hindered diffusion of the $AuCl_4$/CTAB complex to the gold core surface, and consequently, a faster decrease in the absorption plasmon band.

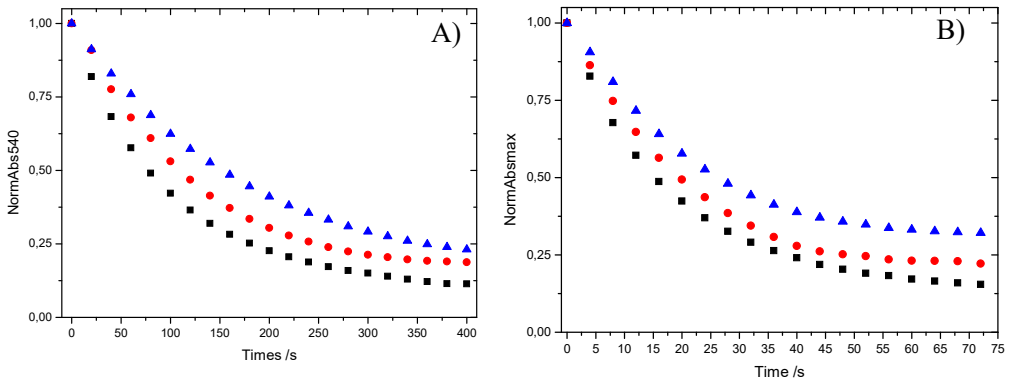

Figure 3. Normalized Au absorption plasmon band with respect to oxidation time for 5% (black squares), 10% (red circles) and 15% (blue triangles) at A) 25ºC and B) 50ºC. Each data point is the average of three UV-vis measurements

From the data in Figure 3A, we have determined two parameters; *i)* the Au etching rate and the *ii)* etching $AuCl_4$/CTAB coefficient diffusion. These parameters have been previously investigated for pNIPAM and conductive polymers coated AuNPs, respectively[25,33]. In this work, we have determined both parameters at 3 different cross-linking densities (5%, 10% and 15%) and at the two possible microgel states (swollen and collapsed). The Au etching rate was obtained by following the same procedure previously used by Lyon et al.[25] This value was obtained by fitting the plot of the normalized absorption plasmon band decrease in function of time. Figure 4 (black squares) and Table 2 show the etching rates values for Au core oxidation in Au@pNIPAM at 5, 10 and 15% BA at 27ºC. As shown, the values of the gold oxidation rate decrease as the amount of crosslinker into the microgel network increases, 1.01×10^{-2}, 8.9×10^{-3} and 6.4×10^{-3} s^{-1}. This means a decrease (in %) from 5 to 15% BA of 37%. Is important to mention that our etching rate values are in the same order of magnitude

that those obtained by Lyon et al. for the Au oxidation in Au@pNIPAM-co-AAc particles with different shell thickness using KCN.[25]

We have also determined etching rates values for the three Au@pNIPAM systems when the microgel is in the collapsed state. Figure S2 includes time evolution of the UV-vis absorption plasmon band during Au oxidation for Au@pNIPAM particles with 5%, 10% and 15%. The peaks corresponding to the Au absorption plasmon band as well as the peak for the $AuCl_4$/CTAB complex are again observed. However, compared with the oxidation at low temperature, the time needed to completely oxidize the gold core is reduced to ~70 min. These result agree with those found by Lyon et al. for Au@pNIPAM-co-AAc with different shell thickness at 25 and 45ºC temperatures.[25] Figure 3B represents the decrease of the normalized plasmon band absorbance in function of time for the 3 different cross-linking percentages at 50ºC. Again, even if the microgel remains in the collapsed state, the Au oxidation kinetics depends on the cross-linker percentage within the microgel network, Calculated etching rate values (extracted from fitting the plot of figure 3B) are included in Figure 4 (red circles) and table 2. As is observed, etching rates decrease as the cross-linker amount is increased, with values $5.4x10^{-2}$, $4.9x10^{-2}$ and $4.4x10^{-2}$ s^{-1} for 5, 10 and 15% BA, respectively. However, the decrease (in %) in the etching rate values for 5 and 15% at 50ºC was 18%, lower compared with those obtained at 27ºC. Importantly, if we compare the etching rates at both measured temperatures, the values at 50ºC are almost one order of magnitude higher compared with those at 27ºC. As expected from Arrhenius' law, the oxidation rate increases with temperature,[40] and it was able to compensate that the microgel was in the collapsed state. This increase in the etching rate values with temperature are in concordance with those values previously obtained by Lyon et al.[25]

Table 2. Etching rates for Au oxidation at 27 and 50ºC for Au@pNIPAM with 5, 10 and 15% BA.

Temperature	Etching rate (s^{-1}) 5%BA	Etching rate (s^{-1}) 10%BA	Etchting rate (s^{-1}) 15%BA
27ºC	$1{,}01x10^{-2}$	$8{,}9x10^{-3}$	$6{,}41x10^{-3}$
50ºC	$5{,}4x10^{-2}$	$4{,}9x10^{-2}$	$4{,}4x10^{-2}$

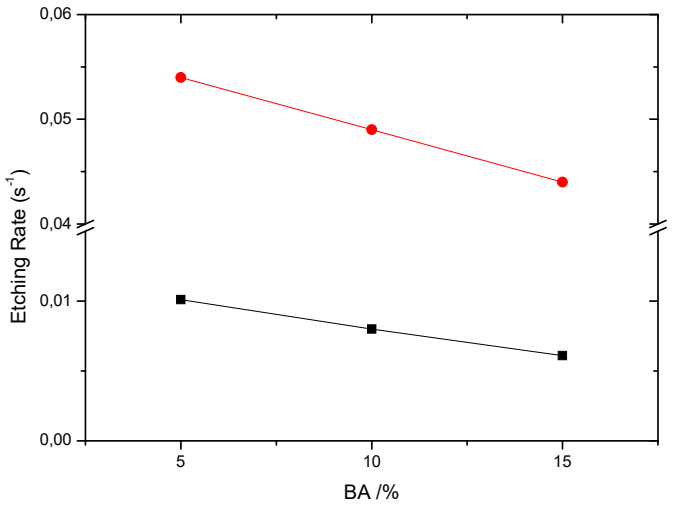

Figure 4. Etching rates of Au cores at 25ºC (black squares) and 50ºC (red circles) for Au@pNIPAM particles at 5, 10 and 15% BA.

Apart from the etching rates values, we have also obtained the $AuCl_4$/CTAB diffusion coefficient for the three hybrid systems. This parameter was determined using the same method than the previously reported by Feldheim et al.[33] They investigated the diffusion coefficient for KCN during the oxidation of spherical AuNPs coated by a conductive polypyrrole shell.[33] In this investigation, they followed a model for diffusion in a sphere:

$$1 - (C_t - C_0)/(C_s - C_0) = b \exp(-At); \text{ with } A = D\pi^2/L^2 \quad [2]$$

where C_t is the concentration of diffusing species at time t, C_s is surface concentration, C_0 is the diffusant coefficient at the film/particle interface a t=0, and b is a constant

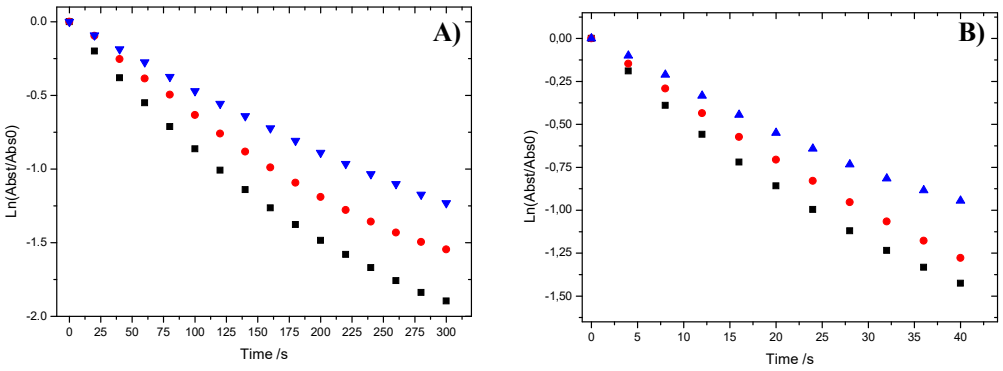

Figure 5. Fit from the absorption plasmon band intensity values in function of time for the diffusion in a spherical polymer for Au@pNIPAM with 5% (black square), 10% (red circle) and 15% (green triangle) at A) 27ºC and B) 50ºC.

dependent on the initial boundary conditions employed in solving Fick´s law. Under these experimental conditions, C_0 may be set to 0, and eq. 2 can be related to the gold plasmon band intensity:

$$(abs_t/abs_0) = b \exp(-At) \qquad [3]$$

where abs_0 and abs_t are the gold plasmon absorbances intensities before gold etching and at a certain time during oxidation reaction, respectively. Figure 5A and 5B represents the fit of the absorption plasmon band intensities during gold oxidation corresponding to the 3 different cross-linking densities below and above phase transition, respectively. Table 3 includes diffusion coefficient values at 27 and 50ºC, where D_h is the hydrodynamic diameter obtained by DLS analysis, and L represents the shell thickness, calculated as $(D_h - 50)/2$. As was expected, the $AuCl_4$/CTAB diffusion coefficient decreases as the cross-linker percentage is increased, $7.7x10^{-12}$, $2.57x10^{-12}$

and $1.12x10^{-12}$ cm^2/s for 5, 10 and 15% cross-linker, respectively. The decrease is now 85.5%. These values are in the same order of magnitude than those obtained by Feldheim et al.[33] Diffusion coefficients have been also calculated for the AuNPs oxidation at 50ºC for the 3 cross-linking values (Figure 5B and Table 3). In this case, as the microgel is in the collapsed state, L values are lower compared with those at 27ºC (see table 3). As expected, at 50ºC diffusion coefficients decrease as the cross-linker increases, being $6.0x10^{-13}$, $2.3x10^{-13}$ and $1.9x10^{-13}$ cm^2/s for 5, 10 and 15% BA, respectively. The decrease in this case is 68,3%. These values suggest that as the microgel network is in a "hydrophobic" environment it causes a less favorable diffusion of $AuCl_4$/CTAB complex towards the Au surface. On contrary that in the previous etching rates values (see values above), diffusion coefficients are one order of magnitude lower at 50ºC compared with those at 27ºC. Indeed, Figure 6 shows the lower dependence in the cross-linking percentage in etchant diffusion at both measured temperatures.

Table 3. Hydrodynamic diameter (D_h), shell thickness (L) and etchant diffusion coefficient for Au@pNIPAM microgels with 5, 10 and 15% BA.

Cross-linker	**5%BA**	**10%BA**	**15%BA**
D_h (27ºC) /nm	460	435	412
L (27ºC) /nm	205	192,5	181
D (27ºC)/cm^2/s	**$7,07x10^{-12}$**	**$2,57x10^{-12}$**	**$1,12x10^{-12}$**
D_h (50ºC) /nm	211	211	211
L (50ºC) /nm	80,5	80,5	80,5
D (50ºC)/cm^2/s	**$6,00x10^{-13}$**	**$2,33x10^{-13}$**	**$1,9x10^{-14}$**

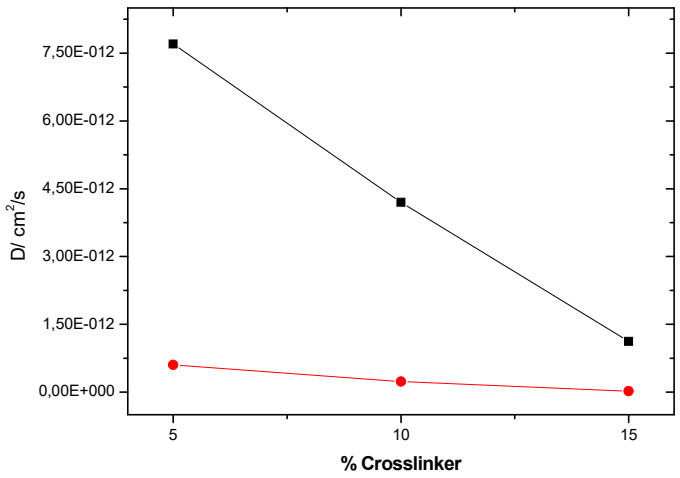

Figure 6. Diffusion coefficient for Au@pNIPAM at 5, 10 and 15% BA at 27ºC (black square) and 50ºC (red circles).

3.3 Fabrication of Au@p4VP and hollow p4VP particles.

Figure 7 includes TEM images of the hybrid Au@p4VP systems at 3 BA contents. Surprisingly, unlike the previous Au@pNIPAM system, the Au core is not exactly located at the center of the hybrid Au@p4VP structure.[38] This situation indicates that for 4VP monomer, the polymerization is not homogeneously produced surrounding the AuNP surface. We hypothesize that as the polymerization process was performed at water pH (pH~6) the 4VP monomer is mainly not protonated, and consequently hydrophobic. On contrary, the CTAB molecules attached on the Au surface in form of bilayers are positively charged,[37] which can be considered that are hydrophilic. For this reason we believe that the tendency of the polymer to grow surrounding the hydrophilic Au surface is not favorable here, due to the different hydrophobic-hydrophilic nature between polymer and Au surface, i.–e. once the 4VP starts to polymerize on the Au surface, the monomer has more affinity in growing through itself that surrounding the AuNPs surface, thus resulting in a "Janus" hybrid structure.

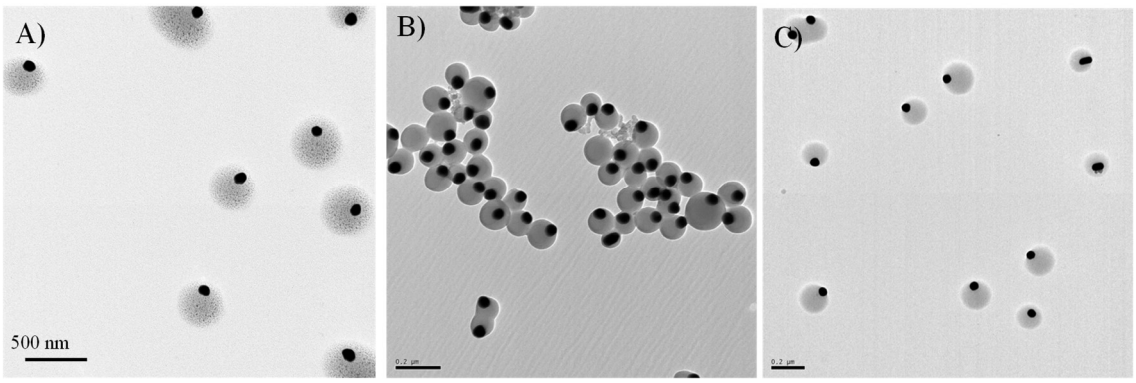

Figure 7. Representative TEM images of Au@p4VP particles at A) 5%, B) 10% and C) 15% BA.

This "Janus" system was also introduced in an $AuCl_4$/CTAB mixture to induce gold oxidation. Figure 8A and 8B show representative TEM images of the Au@p4VP at 10% BA after complete Au oxidation. As expected, the hollow is located in the same position where the metal gold was positioned before oxidation. This means that the oxidation is differently achieved if it is compared with Au@pNIPAM system. For the thermo-responsive microgel, the Au core was located at the center of the polymer shell, consequently, the oxidation is produced by homogeneous diffusion of the $AuCl_4$/CTAB complex through the microgel network. However, for the Au@p4VP system, we can easily deduce that the $AuCl_4$/CTAB complex can firstly reach the Au surface by the no-coated part instead through the polymer-coated part (across the p4VP microgel). Figure 8C includes a graphical representation of the 2 possible oxidation approaches, which we have denoted as a *direct-like* oxidation or an *across-like* oxidation. The most plausible mechanism would be the direct oxidation, as is faster due to the total or partial absence of polymeric hindrance. In order to explain the most probable oxidation approach, we have calculated the gold etching rate in each case.

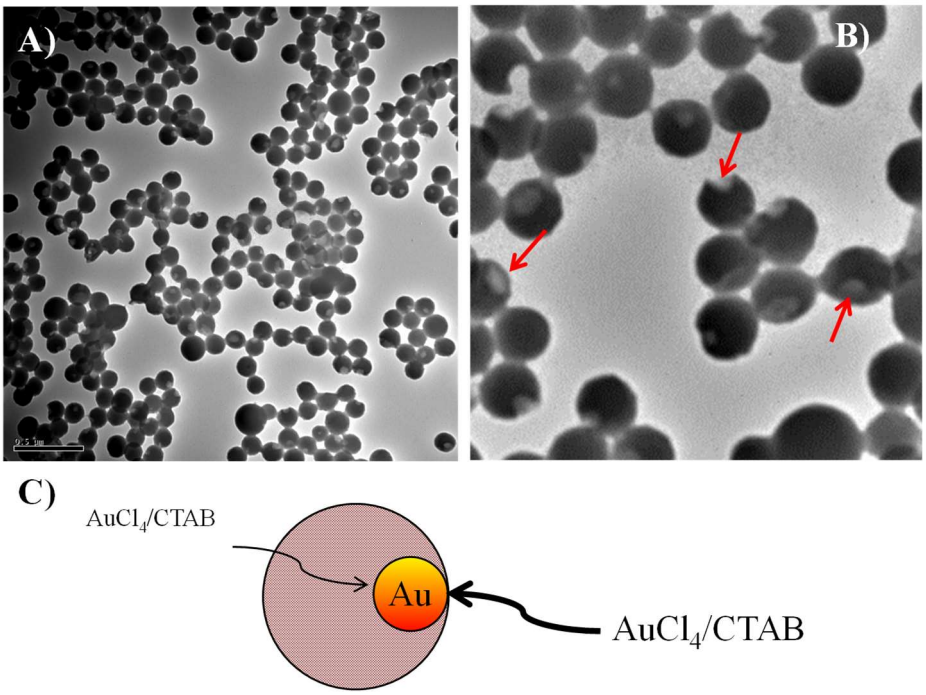

Figure 8. A) and B) Representative TEM images of hollow p4VP particles at 10% BA at different magnification (the hollow is showed with a red arrow). C) Schematic representation for the 2 possible oxidation routes in Au@p4VP particles

3.4 Gold etching rate and $AuCl_4$/CTAB coefficient diffusion

We have investigated the gold core oxidation for this hybrid "Janus" system. As was previously mentioned, p4VP presents two different states below and above pH ~ 4.8. Below this pH value nitrogen atoms are protonated, the repulsive forces causes a microgel swells and water molecules can diffuse into the microgel network. Above this pH value nitrogen groups are deprotonated, and the hydrophobic forces become dominant, thus promoting a microgel collapse. For this reason, we have investigated the gold core oxidation at three cross-linking densities (5, 10 and 15%) and at pH 2 and pH 7. The gold oxidation process was again monitored by UV-vis spectroscopy. Figure S3 shows time evolution of the UV-vis absorption spectrum during Au oxidation for Au@p4VP with 5%, 10% and 15% BA at pH 2 (swollen state). The two UV-vis peaks

were again observed, with a decrease in the plasmon band intensity as metal core oxidation is performed. However, the total oxidation was produced at about 600 minutes of reaction, which is higher compared with that for Au@pNIPAM particles at 27ºC. Figure 9A represents the decrease of the normalized plasmon band absorbance with respect to oxidation time for the 3 different cross-linking percentages, 5% (black square), 10% (red circles) and 15% (blue triangles) at pH 2. As shown, Au oxidation did not depend on the cross-linking density within the microgel network, contrary to the the Au@pNIPAM case (Figure 3). For Au@p4VP particles, a decrease in the BA content into the polymer network during Au oxidation resulted in a similar plasmon absorbance decrease. This tendency was confirmed by obtaining the etching rate at each cross-linking density. This value was obtained by fitting the plot of the normalized absorption plasmon band decrease in function of time. Table 4 and Figure 10 include the etching rates values for the Au core oxidation using Au@p4VP at 5, 10 and 15% BA at pH 2. As shown, the etching rate values were almost constant with the amount of crosslinker. This value minimally increased from $6.8x10^{-3}$, $6.3x10^{-3}$ and $5.4x10^{-3}$ s^{-1} for microgles with 5%, 10% and 15% BA, respectively, only 20% decrease. In the same way, concerning etching rates values at pH 7 (Table 4 and Figure 10) almost equal values were obtained at 3 different cross-linking densities. This minor variation in the etching rate values means that the etchant diffusion is almost totally produced by the non-coated part, and a minor complex diffusion is achieved through the p4VP shell. These values were 4.8x10-3, 4.7x10-3 and 4.6x10-3 s-1 fro 5, 10 and 15% BA. This means a 4,2% of decrease.

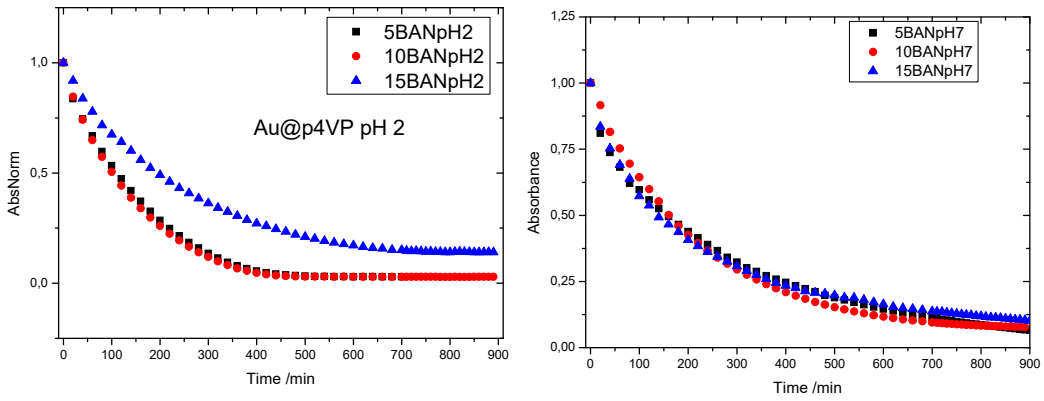

Figure 9. Normalized Au absorption plasmon band with respect to oxidation time for Au@p4VP with 5% (black squares), 10% (red circles) and 15% (blue triangles) at A) pH 2 and B) pH 7

We would like to remark that in the previous Au@pNIPAM system the diffusion coefficient was calculated by the same approach previously used by Feldheim et al. This parameter was obtained by following a model for diffusion in a sphere[33]. In equation 2, $A=D\pi^2/L$, being L the shell thickness, calculated as $(D_h - 50)/2$, where Dh is the hydrodynamic diameter. For Au@pNIPAM particles, L can be well-estimated because the Au core is structured in the center of the core@shell system. However, as TEM images demonstrated, the Au@p4VP particles had a Janus-like structure. In this specific case, the shell thickness can not be estimated by the same approach, as the gold core is not located in the center of the core@shell system. Apart from that, calculated etching rate values confirmed that the oxidation is carried out by the non- or less-coated part of the Au core. For these reason, we have not calculated the $AuCl_4$/CTAB diffusion coefficient for Au@p4VP particles.

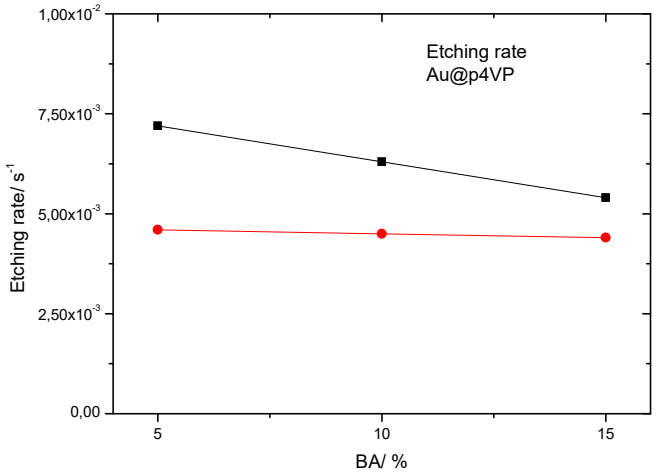

Figure 10. Etching rates of Au cores at pH 2 (black squares) and pH 7 (red circles) for Au@p4VP particles at 5, 10 and 15% BA

To support our hypothesis that the Janus structure in the Au@p4VP system is produced due to the different hydrophilicity between monomer and Au surface, we have carried out the polymerization in presence of a hydrophilic co-monomer, methyl methacrylate (MMA). We have used MMA because it is a hydrophilic monomer that do not provide stimuli-responsive behavior, as is supplied for other commonly used hydrophilic co-monomers, as acrylic acid, allylamine, or butenoic acid. In our investigations polymerized 4VP in presence of increased amounts of MMA. Figure 11 include TEM images for Au@p4VP with 5, 10, 20 and 25% MMA. As is observed, the Janus morphology disappeared even in the sample with the lower amount of MMA, and the Au core is more centered as the amount of MMA is augmented. Interestingly, TEM images also show an increase in the microgel diameter with the MMA content. Table 4 includes average microgel size (measured by TEM images) and hydrodynamic diameter for Au@p4VP systems with MMA. As is observed the microgel size increases with the amount of MMA in the polymerization mixture.

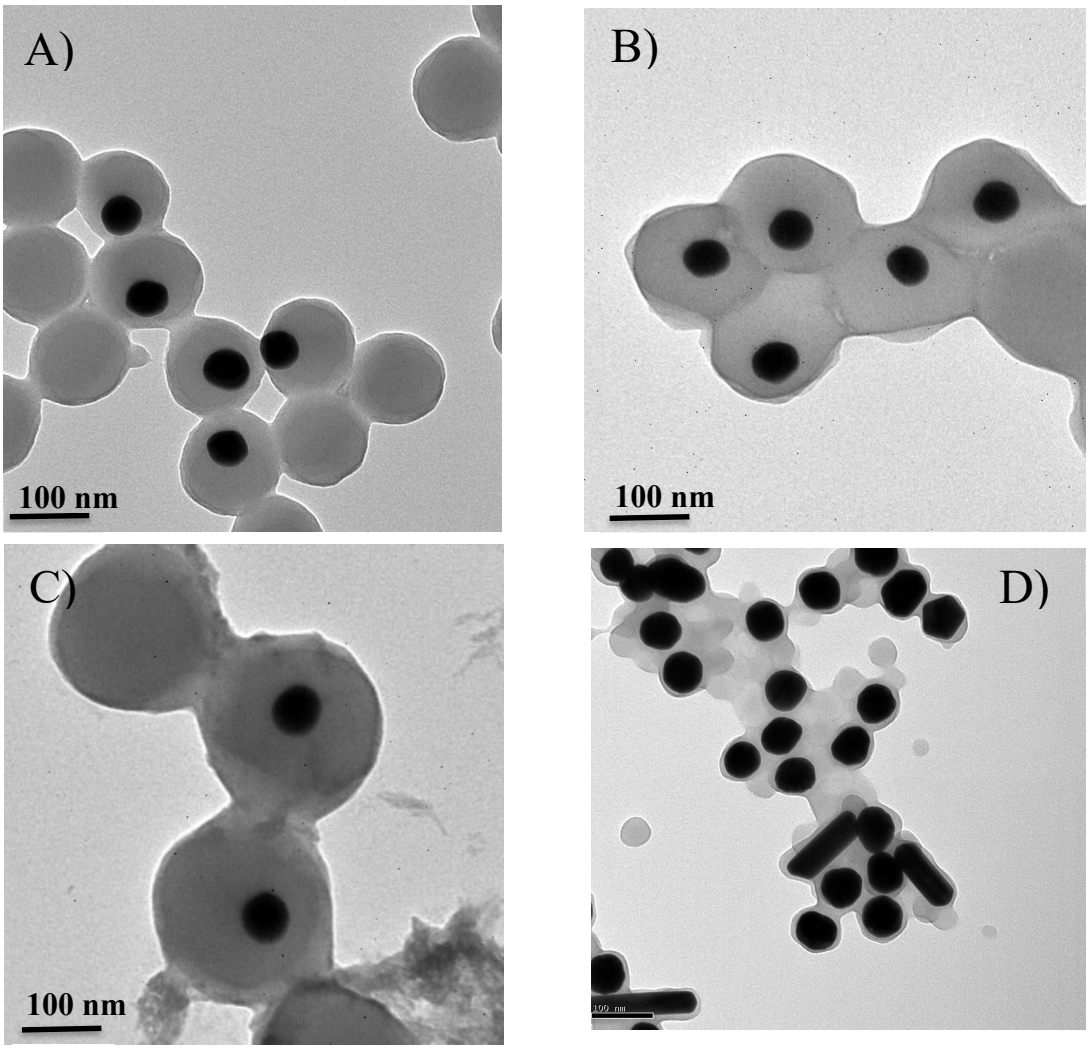

Figure 11. Representative TEM images of the Au@p4VP samples with A) 5%, B)10%, C) 20% and D) 25% MMA

Table 4. Average particles size and DLS for Au@p4VP with different amount of MMA.

MMA (%)	Size /nm (TEM)	Dh /nm (DLS)
5	130 ± 10	
10	139 ± 11	
20	177 ± 12	

FALTAN LOS DH

4. Conclusions

In conclusion, we have performed the synthesis of hybrid Au@pNIPAM and Au@4VP particles for the fabrication of hollow thermo-and pH-responsive pNIPAM and p4VP microgels. The Au core elimination was performed by easily $AuCl_4$/CTAB diffusion through the microgel network. Initially, TEM characterization demonstrated the hybrid nature and the morphology of the core@shell as well as the hollow structure and confirmed that hybrid systems did not have the same polymeric structuration. The spherical AuNP was centered into the core@shell structure for thermo-responsive microgels. However, a Janus morphology was observed for Au@p4VP particles. Importantly, this structure was maintained after gold core elimination. We hypothesize that there is a low tendency of the hydrophobic 4VP monomers to polymerize surrounding the hydrophilic Au particles. A detailed investigation of the Au oxidation was performed by using particles with 5, 10 and 15% BA cross-linking at 27 and 50ºC for Au@pNIPAM and at pH 2 and 7 for Au@p4VP microgels. A decrease of both etching rates values and $AuCl_4$/CTAB diffusion coefficient were observed for Au@pNIPAM particles as the BA amount into the microgel network was increased. Due to the Arrhenius law obtained etching rates values were higher above the pNIPAM phase transition. However, diffusion coefficients were lower when the oxidation process was performed at the collapsed state. This crosslinker-dependant behavior remarkably changed for Au@p4VP particles. In this case etching rates values were almost independent of the BA amount below and above the phase transition. The Janus-like morphology causes that the diffusion of the $AuCl_4$/CTAB complex was mainly produced through the non- or- less coated area. Finally, we have fabricated Au@p4VP system with a centered Au core by introducing a hydrophilic co-monomer during the polymerization process. The presented investigation can be used for the fabrication of

hybrid microgels with tunable accumulation or release capability that can be applied in biomedical applications.

Acknowledgements

The authors acknowledge financial support from the Spanish MINECO projects ~~CTQ2013-48418P and~~ CTQ2016-76311-R. RCC acknowledge funding from the Comunidad de Madrid for the Atraccion de Talento Investigador project (2018-T1/IND-10736).

Supporting Information

Time evolution of the UV-vis absorption spectrum during Au oxidation at 27ºC for Au@pNIPAM at 5%, 10% and 15% cross-linking, respectively.

Author information

Corresponding author: R.C.C. rcontreras@uma.es

Author Contributions

The manuscript was written through contributions of all authors. All authors have given approval for the final version of the manuscript.

Notes

The authors declare no competing financial interest.

References

[1] Zelikin, A. N.; Li, Q.; Caruso, F. Disulfide-estabilized poly(methacrylic acid) capsules: formation, cross-linking, and degradation behaviour. *Chem. Mater*. **2008**, 20, 2655-2661.

[2] Levy, T.; Déjugnat, C.; Sukhorukov, G. B. Polymer micro-capsules with carbohydrate-sensitive properties. *Adv. Funct. Mater.* **2008**, 18, 1586-1594.

[3] Kozlovskaya, V.; Kharlampieva, E.; Mansfield, M. L.; Sukhishvili, S. A. Poly(methacrylic acid) hydrogel films and capsules: Response to pH and ionic strength, and encapsulation of macromolecules. *Chem. Mater.* **2005**, 18, 328-336.
[4] Peyratout, C. S.; Dähne, L. Tailor-made polyelectrolyte microcapsules: from multilayers to smart containers. *Angew. Chem., Int. Ed.* **2004**, 43, 3762-3783.
[5] Agrawal, G.; Agrawal, R.; Pich, A. Dual responsive poly(N-vinylcaprolactam) based degradable microgels for drug delivery. *Part. Part. Syst. Charact.* **2017**, 34, 1700132.
[6] Liu, L.; Zeng, J.; Zhao, X.; Tian, K.; Liu, P. Independent temperature and pH dual-responsive PMAA/PNIPAM microgels as drug delivery system: Effect of swelling behavior of the core and shell materials in fabrication process. *Colloids Surf. A: Physicochem. Eng. Aspects* **2017**, 526, 48-55.
[7] Wang, Y.; Nie, J.; Chang, B.; Sun, Y.; Yang, W. Poly(vinylcaprolactam)-Based biodegradable multiresponsive microgels for drug delivery. *Biomacromolecules* **2013**, 14, 3034-3046.
[8] Smeets, N. M. B.; Hoare, T. Designing responsive microgels for drug delivery applications. *Journal of Polymer Science, Part A: Polymer Chemistry* **2013**, 51, 3027-3043.
[9] Vinogradov, S. V. Colloidal microgels in drug delivery applications. *Current Pharmaceutical Design* **2006**, 12, 4703-4712.
[10] Schild, H. G. Poly(N-isopropylacrylamide): Experiment, theory and application. *Prog. Polym. Sci.* **1992**, 17, 163-249.
[11] Sawai, T.; Yamazaki, S.; Ikariyama, Y.; Aizawa, M. pH-Responsive swelling of the ultrafine microsphere. *Macromolecules* **1991**, 24, 2117-2118.
[12] Tanaka, T.; Fillmore, D.; Sun, S.- T.; Nishio, I.; Swislow, G.; Shah, A. Phase Transitions in Ionic Gels. *Phys. Rev. Lett.* **1980**, 45, 1636-1639.
[13] McPhee, W.; Tam, K. C.; Pelton, R. Poly(N-isopropylacrylamide) latices prepared with sodium dodecyl sulfate. *J. Colloid Interface Sci.* **1993**, 156, 24-30.
[14] Suzuki, A.; Tanaka, T. Phase transition in polymer gels induced by visible light. *Nature* **1990**, 346, 345-347.
[15] Pelton, R. H.; Chibante, P. Preparation of aqueous lattices with N-isopropylacrylamide. *Colloids Surf.* **1986**, 20, 247-256.
[16] Peng, X.; Shen, J. Water-soluble copolymers. I. Biodegradability and functionality of poly[(sodium acrylate)-co-(4-vinylpyridine)]. *J. Appl. Pol. Sci.* **1999**, 71, 1953-1957.
[17] Akamatsu, K.; Shimada, M.; Tsuruoka, T.; Nawafune, H.; Fujii, S.; Nakamura, Y. Synthesis of pH-responsive nanocomposite microgels with size-controlled gold nanoparticles from ion-doped, lightly cross-linked poly(vinylpyridine). *Langmuir* **2010**, 26, 1254-1259.
[18] Kim, K. S.; Vincent, B. pH and temperature-sensitive behaviors of poly(4-vinylpyridine-co-N-isopropylacrylamide) Microgels. *Polym. J.* **2005**, 37, 565-570.
[19] Liu, G.; Zhu, C.; Xu, J.; Xin, Y,; Yang, T.; Li, J.; Shi, L.; Guo, Z.; Liu, W. Thermo-responsive hollow silica microgels with controlled drug release properties. *Colloids and Surfaces, B: Biointerfaces* **2013**, 111, 7-14.
[20] Chen, Y.; Chen, Y.; Nan, J.; Wang, C.; Chu, F. Hollow poly(N-isopropylacrylamide)-co-poly(acrylic acid) microgels with high loading capacity for drugs. *Journal of Applied Polymer Science **2012***, 124, 4678-4685.
[21] Liu, X.; Yang, J.; Zha, L.; Jiang, Z. Self-assembly of hollow PNIPAM microgels to form discontinuously hollow fibers. *Chinese Journal of Polymer Science* **2014**, 32, 1544-1549.

[22] Zha, L.; Zhang, Y.; Yang, W. L.; Fu, S. K. Monodisperse temperatura-sensitive microcontainers. *Adv. Mater.* **2002**, 14, 1090-1092.
[23] Lapeyre, V.; Renaudie, N.; Dechezelles, J. F.; Saadaoui, H.; Ravaine, S.; Ravaine, V. Multiresponsive hybrid microgels and hollow capsules with a layered structure. *Langmuir* **2009**, 25, 4659-4667.
[24] Xing, Z.; Wang, C.; Yan, J.; Zhang, L.; Li, L.; Zha, L. pH/temperature dual stimuli-responsive microcapsules with interpenetrating polymer network structure. *Colloid Polym. Sci.* **2010**, 288, 1723-1729.
[25] Singh, N.; Lyon, L. A. Au nanoparticle templated synthesis of pNIPAm nanogels. *Chem. Mater.* **2007**, 19, 719-726.
[26] Zhang, Y.; Jiang, M.; Zhao, J.; Ren, X.; Chen, D.; Zhang, G. A novel route to thermosensitive polymeric core-shell aggregates and hollow spheres in aqueous media. *Adv. Funct. Mater.* **2005**, 15, 695-699.
[27] Wu, S.; Kaiser, J.; Drechsler, M.; Ballauff, M.; Lu, Y. Thermosensitive Au-PNIPA yolk-shell particles as "nanoreactors" with tunable optical properties. *Colloid Polym. Sci.* **2013**, 291, 231-237.
[28] Wu, S.; Dzubiella, J.; Kaiser, J.; Dreschsler, M.; Guo, X.; Ballauff, M.; Lu, Y. Thermosensitive Au-PNIPA yolk-shell nanoparticles with tunable selectivity for catalysis. *Angew. Chem., Int. Ed.* **2012**, 51, 2229-2233.
[29] Contreras-Cáceres. R.; Schellkopf, L.; Fernández-López, C.; Pastoriza-Santos, I.; Pérez-Juste, J.; Stamm, M. Effect of the cross-linking density on the thermoresponsive behavior of hollow Pnipam microgels. *Langmuir.* **2015**, 31, 1142-1149.
[30] Rodríguez-Fernández, J.; Pérez-Juste, J.; Mulvaney, P.; Liz-Marzán, L. M. Spatially-directed oxidation of gold nanoparticles by Au(III)-CTAB complexes. *J. Phys. Chem. B* **2005**, 109, 14257-14261.
[31] Liu, F.; Eisenberg, A. Preparation and pH triggered inversion of vesicles from poly(acrylic acid)-block-polystyrene-block-poly(4-vinyl Pyridine). *J. Am. Chem. Soc.* **2003**, 125, 15059-15064.
[32] Contreras-Cáceres, R.; Leiva, M. C.; Ortiz, R.; Díaz, A.; Perazzoli, G.; Casado-Rodríguez, M. A.; Melguizo, C.; Baeyens, J. M.; López-Romero, J. M.; Prados, J. Paclitaxel-loaded hollow-poly(4-vinylpyridine) nanoparticles enhance drug chemotherapeutic efficacy in lung and breast cancer cell lines. *Nano Research.* **2017**, 10, 856-875.
[33] Marinakos, S. M.; Novak, J. P.; Brousseau III, L. C.; House, A. B.; Edeki, E. M.; Feldhaus, J. C.; Feldheim, D. L. Gold particles as templates for the synthesis of hollow polymer capsules. Control of capsule dimensions and guest encapsulation. *J. Am. Chem. Soc.* **1999**, 121, 8518-8522.
[34] Contreras-Cáceres, R.; Pastoriza-Santos, I.; Álvarez-Puebla, R. A.; Pérez-Juste, J.; Fernández-Barbero, A.; Liz-Marzán, L. M. Growing Au/Ag nanoparticles within microgel colloids for improved SERS detection. *Chem.-Eur. J.* **2010**, 16, 9462-9467.
[35] Turkevich, J.; Stevenson, P. C.; Hillier, J. A study of the nucleation and growth processes in the synthesis of colloidal gold. *Discuss. Faraday Soc.* **1951**, 11, 55-75.
[36] Contreras-Cáceres R.; Sánchez-Iglesias, A.; Karg, M.; Pastoriza-Santos, I.; Pérez-Juste, J.; Pacifico, J.; Hellweg, T.; Fernández-Barbero, A.; Liz-Marzán, L. M. Encapsulation and growth of gold nanoparticles in thermoresponsive microgels. *Adv. Mater.* **2008**, 20, 1666-1670.
[37] Contreras-Cáceres R.; Pacifico, J.; Pastoriza-Santos, I.; Pérez-Juste, J.; Fernández-Barbero, A.; Liz-Marzán, L. M. Au@pNIPAM thermosensitive nanostructures: Control

over shell cross-linking, overall dimensions, and core growth. *Adv. Funct. Mater.* **2009**, 19, 3070-3076.

[38] Clara-Rahola, J.; Moscoso, A.; Ruiz-Muelle, A. B.; Laurenti, M.; Formanek, P.; Lopez-Romero, J. M.; Fernández, I.; Diaz, J. F.; Rubio-Retama, J.; Fery, A.; Contreras-Cáceres, R. Au@p4VP core@shell pH-sensitive nanocomposites suitable for drug entrapment. *J. Colloid Interface Sci.* **2018**, 514, 704-714.

[39] Flory, P.J. *Principles of Polymer Chemistry*; Cornell University Press: Ithaca, NY, **1953**.

[40] Carregal-Romero, S.; Pérez-Juste, J.; Hervés, P.; Liz-Marzán, L. M.; Mulvaney, P., Colloidal Gold-Catalyzed Reduction of Ferrocyanate (III) by Borohydride Ions: A Model System for Redox Catalysis. *Langmuir* **2010,** 26, 1271-1277.